RF Metasurface Array Design Using Deep Convolutional Generative Adversarial Networks

John A. Hodge[1], Kumar Vijay Mishra[2] and Amir I. Zaghloul[1,2]

[1]Bradley Department of Electrical and Computer Engineering, Virginia Tech, Falls Church, VA 22043 USA
[2]United States CCDC Army Research Laboratory, Adelphi, MD 20783 USA
Email: {[1]jah70, [3]amirz}@vt.edu, [2]kumarvijay-mishra@uiowa.edu

***Abstract*—In recent years, metasurface (MTS) arrays have shown promising abilities to control and manipulate electromagnetic (EM) waves through modified surface boundary conditions. The constituent unit elements of a MTS have become increasingly complex with rise of anisotropic radio-frequency (RF) applications such as beam scanning through anomalous reflection/refraction, beam focusing, and polarization conversion in an extremely low-profile. Designing these meta-atoms or metagratings is a challenging and time-consuming procedure. Each new MTS design typically requires numerous iterations of manual tuning and full-wave simulations. In this paper, we employ deep convolutional generative adversarial networks (DC-GANs) to generate anisotropic RF metamaterial unit cell designs for MTS arrays. Using a small set of simulated meta-atom spectra, these networks learn the relationship between the physical structure of meta-atoms and their reflection spectra for vertical and horizontal polarizations. Our numerical experiments demonstrate that DC-GANs are able to generate meta-atom structures that resemble design features in the training data. Numerical experiments with design test case showed 90% accurate reflection responses with errors within 0.2 (1.3) dB in magnitude and 3.0° (4.4°) in phase for the co-polar (cross-polar) component.**

***Index Terms*—deep learning, generative adversarial networks, inverse design, metasurfaces, radiation pattern**

I. Introduction

Metasurfaces (MTSs) have garnered significant interest in the antenna community in recent years [1]. This is largely because of their ability to control and manipulate electromagnetic waves in sub-wavelength thickness through modified boundary conditions [2]. The MTS is a two-dimensional equivalent of metamaterials, which are composed of electrically thin and densely packed planar arrays of resonant or nearly resonant subwavelength elements [3]. Electromagnetic properties and functionalities of MTSs are defined by the structure and specific features of their subwavelength unit cell elements or *meta-atoms*. The meta-atoms are periodic subwavelength metal-dielectric structures that resonantly couple with the electric and/or magnetic components of the incident electromagnetic fields, exhibiting properties that are not found in nature [4, 5].

The unusual, interesting behavior of MTS in a low-profile has been proposed to tailor EM waves for many practical radio-frequency (RF) systems that require constrained beam-pattern design such as radar and communications [6]. Typically, design procedure of MTS entails iteratively solving Maxwell's equations through a lot of trial-and-error in a full-wave electromagnetic (EM) simulator by an experienced researcher, thereby imposing prohibitive costs on time, resources and computations (see e.g. [7] for an overview). To realize the full potential of MTSs for practical applications, more automated design techniques are required. In this context, recent research suggests use of machine learning (ML) to mitigate the costs involved and make MTS design accessible to a wider range of engineers [8]. As a class of ML methods, deep learning (DL), which employs artificial neural networks with many connected layers, has captured much interest recently for solving many challenging problems such as speech, image, and language processing [9, 10]. In particular, design of antennas based on deep networks has recently been demonstrated in traditional array designs [11, 12].

When applied to MTS design problem, DL networks have the advantage of learning intricate, non-intuitive relationships between a metamaterial surface structure and its EM response through a set of training examples [8]. Using these trained transmission or reflection response data sets, the learning algorithms synthesize a custom-defined, arbitrary wave-front MTS or a *metagrating* [13, 14]. Lately, analogous ML/DL-based approaches are also increasingly applied for inverse design in nanophotonic structures [15–17], chiral metamaterials [8], and anisotropic digital coding MTSs [18].

Very recently, *generative adversarial networks* (GANs) [19] have been proposed to predict new designs of MTS meta-atoms [20] and metagratings [14]. These works do not exploit ML to perform classification or predict design parameters. Instead, they use an example data set to train a deep network to generate data from the same estimated underlying probability distribution. A GAN comprises a discriminator neural network classifier and and a generator neural network. While the former is trained to distinguish between real samples and generated samples, the latter is trained to generate samples that fool the discriminator by injecting a random latent variable. Often CNNs are employed for both generator and discriminator networks. These deep convolutional GANs (DC-GANs) have been shown to improve the overall GAN performance [21].

In a GAN-based MTS design, the DL network accepts desired beam-pattern or spectra as input and produces complex shapes of meta-atoms that meet the specified radiation spectra requirements. These models can learn from dozens or hundreds of training examples and, therefore, are more data efficient than other DL-based MTS design approaches, e.g. using a simple convolutional neural network (CNN). When compared with the excessive time and computational cost involved in producing CNN training examples through a full-wave EM simulation, the generative models offer significant benefit of reduced training examples. Moreover, CNN-based approaches interpolate from large sets of *known* MTS designs to approximate the desired spectra or predict requisite design parameters. In comparison, GAN-based design produces new, *undiscovered* meta-atom patterns.

In this paper, we employ DC-GANs to learn the relationship between the physical structure of meta-atoms and their reflection spectra in two polarizations (vertical and horizontal). We use a relatively small data set of simulated meta-atom spectra for training. Unlike standard DC-GAN, our proposed network includes a separate, simulator convolutional neural network (CNN) that quickly validates the response of the synthesized meta-atom shape without resorting to a full-wave simulation. Prior works on GAN-based MTS design [14, 20] focused on only the amplitude response requirements. They also employed arbitrary shapes, including handwritten digit datasets,

978-1-7281-3049-1/19/$31.00 ©2019 IEEE

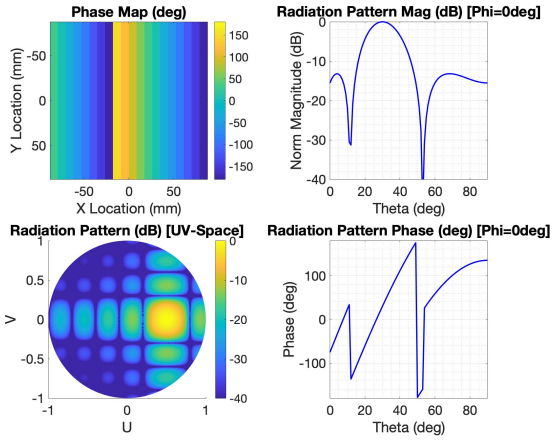

Fig. 1. Top left: Analytical example of a reflect-array MTS comprising sub-wavelength unit cells with a spatially varying phase distribution over the Cartesian x-y plane. The plot shows the phase map of an MTS beam at operating frequency 6 GHz with far-field radiated phase tuned to $+45^{\circ}$. The MTS consisted of 20×20 unit cells with element spacings $d_x = d_y = 8.3$ mm (=$\lambda/6$). Top right: Normalized magnitude of the radiation pattern of a reflected plane wave steered by the MTS to a desired angles $\theta = 30^{\circ}$ and $\phi = 0^{\circ}$. Bottom left: Normalized magnitude of the radiation pattern after steering in the u-v space. Here, $u = \sin\theta\cos\phi$ and $v = \sin\theta\sin\phi$. Bottom left: The corresponding phase of the radiation pattern in the far-field relative to a common phase center [22].

during the training. On the contrary, we design the meta-atoms to meet both amplitude and phase response in co- and cross-polar components. Further, we incorporate various published meta-atom shapes during the training so that the outputs mirror properties of verified patterns in the literature. Our approach demonstrates meta-atom design that meets the spectra requirement in both amplitude, phase, copolar and cross-polar responses. In our previous works, we investigated reconfigurable and electronically active tunable MTS arrays [5, 6, 22–25]. In this paper, for illustration of DL approach, we focus on the design of passive MTS unit cell elements.

In the next section, we describe the system model of MTS meta-atom design. We present our proposed DC-GAN approach in Section III. We validate our methods through simulations in in Section IV before concluding in Section V.

II. MTS Array System Model

MTS arrays are similar to traditional phased arrays in that they are capable of steering an antenna beam to a desired angle and polarization. The far-field radiation pattern of a MTS array is calculated in a similar manner as a conventional phased array. Consider an MTS array with the operating wavelength of the array is λ so that the wavenumber $k = \frac{2\pi}{\lambda}$. Each unit-cell of the MTS lies in the Cartesian plane with dimensions in the x- and y-directions as d_x and d_y, respectively. Further, the entire MTS consists of M and N unit cells in the x- and y-directions, respectively.

The two-dimensional (2-D) reflection amplitude and phase of each MTS unit cell are $a_e(m,n)$ and $\phi_e(m,n)$, respectively, where the indices $m = 1, \cdots, M$ and $n = 1, \cdots, N$ [26]. The far-field phase of each element of the MTS is described in terms of azimuth ϕ and elevation θ angles as

$$\phi_{ff}(m,n) = k\sin\theta((m-1)d_x\cos\phi + (n-1)d_y\sin\phi). \quad (1)$$

From (1), the 2-D far-field radiation pattern of the MTS is

$$f(\phi,\theta) = \sum_{m=1}^{M}\sum_{n=1}^{N} a_e(m,n)\exp\{j(\phi_e(m,n) + \phi_{ff}(m,n)\}. \quad (2)$$

Figure 1 shows an example of the far-field radiation pattern of a beam scanning MTS array using these equations.

Assuming a plane-wave incident illumination, the unit-cell parameters $a_e(m,n)$ and $\phi_e(m,n)$ of the array model in (2) are related to the reflection response vector $\mathbf{R}$ of each meta-atom as

$$a_e(m,n) = |\mathbf{R}| \quad (3)$$

$$\phi_e(m,n) = \angle\mathbf{R}. \quad (4)$$

Usually, the reflection spectral response $\mathbf{R}(\theta_i, f)$ itself is described as a function of the surface admittance tensor $\overline{\overline{\boldsymbol{Y}}}$ [3] of the meta-atom at a particular incidence angle θ_i and frequency f (GHz). In this paper, we fix $\theta_i = 0$ (broadside incidence) so that $\mathbf{R} = \mathbf{R}(\theta_i = 0, f)$, where we have omitted the arguments for simplicity.

The EM wave is also characterized by its polarization. We consider two polarizations - 'x' and 'y' - wherein the electric field is parallel to the x- and y-directions, respectively. For an incident wave with a particular polarization, the MTS produces responses in both polarizations. For example, the response in x (y) polarization when the incident wave is also x-polarized (y-polarized) is the co-polar response $\mathbf{R}_{xx}$ ($\mathbf{R}_{yy}$). Similarly, there are cross-polar responses $\mathbf{R}_{xy}$ and $\mathbf{R}_{yx}$, which we consider identical for passive meta-atoms due to reciprocity. In this paper, our goal is to train the GAN to implicitly learn the relationship of surface admittance tensor $\overline{\overline{\boldsymbol{Y}}}$ with physical meta-atom patterns. Then, the trained network is used to produce meta-atom shapes that realizes the desired composite spectral responses $\mathbf{R}_{xx}$, $\mathbf{R}_{yy}$, $\mathbf{R}_{xy}$, and $\mathbf{R}_{yx}$.

III. DCGAN-Based Metagrating

To realize physical designs for MTS unit cells, we train a DC-GAN to generate patterns of anisotropic MTS unit cells. Figure 2a provides an overview of our DL network architecture. It comprises three DL networks: generator (Fig. 2b), discriminator (Fig. 2c), and simulator (Fig. 2d). This is different than the conventional DC-GAN [21] which consists of only first two networks. The objective of the generator CNN G with network parameters $\boldsymbol{\phi}_g$ is to learn the *generator distribution* $p_{data}(\mathbf{x})$ over the available dataset $\mathbf{x}$. In other words, G maps a prior noise vector $\mathbf{z}$ with distribution $p_{\mathbf{Z}}(\mathbf{z})$ in the latent space and the reflection spectra $\mathbf{R}$ to a (vectorized) image $\mathbf{x}$: $G(\mathbf{z}, \mathbf{R}, \boldsymbol{\phi}_g) \rightarrow \mathbf{x}$. The discriminator $D(\mathbf{x}, \mathbf{R}, \boldsymbol{\phi}_d)$ is also a CNN with network parameters $\boldsymbol{\phi}_d$. This network classifies an image as real (i.e., ≈ 1) or fake (i.e., ≈ 0). The networks G and D interact game-theoretically to find optimal parameter values $\boldsymbol{\phi}_g^*$ and $\boldsymbol{\phi}_d^*$. Here, G generates datasets that closely approximate the normal data distribution $p_{\text{data}}(\mathbf{x})$, and D distinguishes anomalous data from the normal. Following loss function models this interaction [19]

$$V(D,G) = \mathbb{E}_{\mathbf{x}\sim p_{\text{data}}(\mathbf{x})}\left\{\log D(\mathbf{x},\mathbf{R},\boldsymbol{\phi}_d)\right\} + \mathbb{E}_{\mathbf{z}\sim p_{\mathbf{Z}}(\mathbf{z})}\left\{\log(1 - D(G(\mathbf{z},\mathbf{R},\boldsymbol{\phi}_g)))\right\}. \quad (5)$$

978-1-7281-3049-1/19/$31.00 ©2019 IEEE

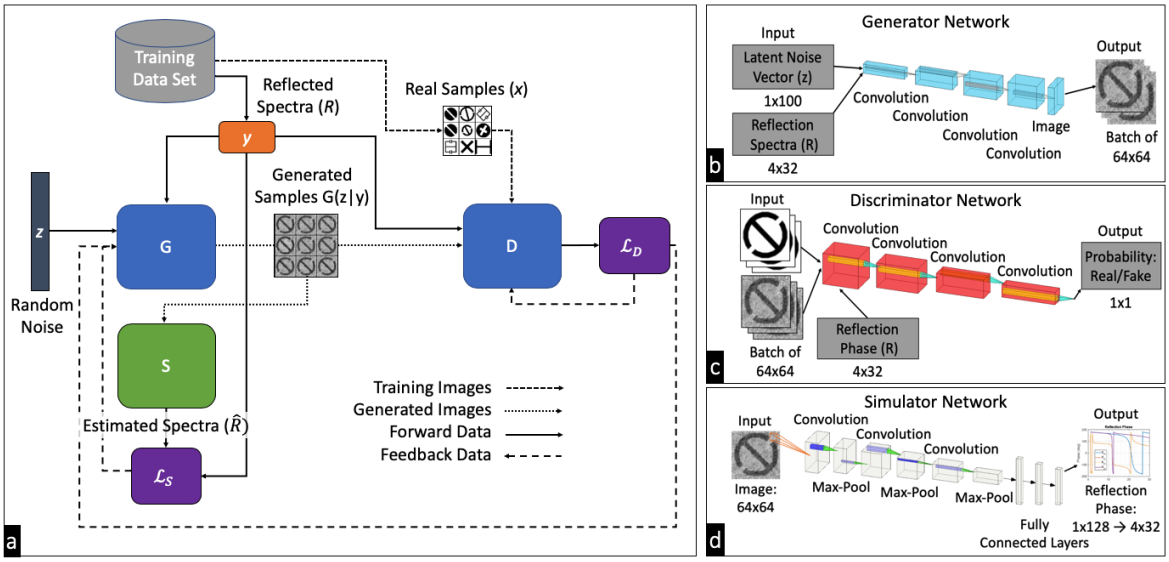

Fig. 2. (a) Overview of the conditional DC-GAN network architecture. The (b) generator (G), (c) discriminator (D), and (d) simulator (S) are CNNs. The S is trained prior to G and D using HFSS simulated reflection phase data over frequency for each meta-atom unit-cell in the training data set. The meta-atom training images are the external conditional input to the DC-GAN. The generated MTS unit-cell design images are the new MTS unit-cell designs output by the GAN. The probability indicates whether D predicts the input is from the training (real) or generated (fake) data sets.

Then, solving the minimax problem

$$\{D^*, G^*\} = \arg\min_G \arg\max_D V(D, G), \tag{6}$$

yields the optimal networks G^* and D^*.

Conventional GANs do not have any controls on the kind of data being generated. This problem is overcome by conditioning G and D on some extra information $\mathbf{R}$ which is provided as an additional input to either or both networks. In this paper, we employ this conditional GAN (cGAN) approach [27] within the DC-GAN architecture. As mentioned earlier, our DC-GAN architecture comprises an additional simulator network S, which approximates the scattering responses $\mathbf{R}_{xx}$, $\mathbf{R}_{yy}$, $\mathbf{R}_{xy}$, and $\mathbf{R}_{yx}$ for a given image matrix that represents the physical structure of the unit cell. Our simulator is a 32-layer CNN that consists of convolutional, batch normalization, leaky ReLU, pooling, dropout and fully-connected layers. The final layer is the regression layer that employs following mean-squared-error (MSE) of the predicted real and imaginary scattering responses at each frequency as its loss function $\mathcal{L}_S$:

$$\mathcal{L}_S = \frac{1}{N}\sum_{i=1}^{N}(\mathbf{R}_i - \hat{\mathbf{R}}_i)^2, \tag{7}$$

where N is the number of predicted response data points, $\mathbf{R}$ is the predicted response vector, and $\hat{\mathbf{R}}$ is the known response obtained through full-wave EM simulations or measurements.

The input to the generator (Fig. 2b) is a random latent noise vector $\mathbf{z}$ and the spectral response from the simulator network over 32 frequency points. This is an example of a cGAN where the spectral response is the extra information $\mathbf{R}$. To allow us to include the spectral response as a conditional input, the loss function of G is modified from the implementation in [28] as

$$\mathcal{L}_G = \gamma \log(D(G(\mathbf{z}, \mathbf{R}, \phi_g)) - \log(\mathcal{L}_S), \tag{8}$$

where γ is a scaling factor parameter to balance the weights of $D(G(\mathbf{z}, \mathbf{R}, \phi_g)$ and $\mathcal{L}_S$.

TABLE I
DC-GAN CNN PARAMETERS.

Network	Input	Output
Simulator (S)	Unit cell design/image	RF reflection spectra
Generator (G)	Latent noise vector, RF reflection spectra	Unit cell design/image
Discriminator (D)	RF reflection spectra, real and generated unit cell designs/images	Decision: real/fake

The discriminator (Fig. 2c) comprises strided convolution layers, batch norm layers, and leaky ReLU activations. In our DC-GAN, the loss function of D is

$$\mathcal{L}_D = \log(D(\mathbf{x}, \phi_d)) + \log(D(G(\mathbf{z}, \mathbf{R}, \phi_g))). \tag{9}$$

In training the DC-GAN, our goal is to maximize $\mathcal{L}_D$ and $\mathcal{L}_G$. Note that this implementation differs from [19], which seeks to minimize $\log(1 - D(G(\mathbf{z}, \mathbf{R}, \phi_g)))$, in an effort to provide sufficient gradients early in the training process. The equilibrium of the minimax training game between G and D arrives when the synthesized output image from the generator is indistinguishable from images directly in the training data set [19]. Then, the content of the generated image represents the physical structure of a meta-atom design. The loss between D and G is calculated using the binary cross entropy (BCE). Table I summarizes all three constituent networks of our proposed DC-GAN.

IV. Numerical Experiments

We validated our proposed approach through simulations. Our training data consisted of 150 metamaterial unit cell designs in a reflect-array configuration. The training data set was generated through full-wave simulation of MTS unit cells using ANSYS HFSS software. Each unit cell was simulated in HFSS with a Floquet port excitation and periodic boundary conditions. The Floquet port allows for transverse electric (TE) and magnetic (TM) excitations to mimic the anisotropic response of the MTS unit cell. In this training data

978-1-7281-3049-1/19/$31.00 ©2019 IEEE

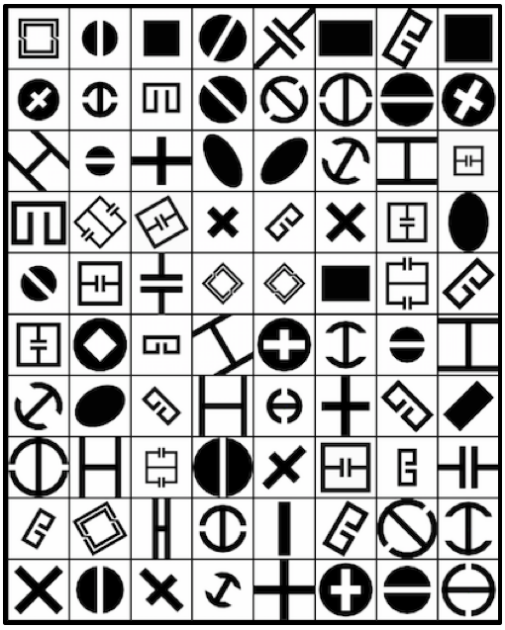

Fig. 3. 80 randomly selected training images of MTS unit cell designs from our design database used to train DC-GAN. The basic shapes are derived from the published literature [1, 29–38].

set, the Floquet port assumes broadside incident plane waves. Each MTS unit cell in the training data set has grid dimensions of 5 mm by 5 mm. Each metamaterial unit cell design 0.5 mm layer of Duroid dielectric ($\epsilon = 2.2, \delta = 0.0009$) with a PEC groundplane beneath the dielectric. The height of the air box is 15 mm, and the Floquet port is de-embedded to the surface of the MTS.

For training, we relied on various published anisotropic MTS unit cell resonator designs [1, 29–38]. As shown in Fig. 3, the training data was generated through multiple variations of each base unit cell design to provide a range of anisotropic magnitude and phase responses across the spectrum of interest (1-30 GHz). We used PyTorch [39] implementation of the binary cross entropy (BCE) loss function and batch normalization for training DC-GAN. An Adam optimizer [40] - a stochastic optimization technique - was used in training both generator and discriminator networks. Simulations were performed using a CPU (central processing unit) with a 2.9 GHz Intel Core i5 processor.

Figure 5 shows the training loss of the DC-GAN over 2000 epochs (iterations). The objective was to maximize G while making $D = 0.5$, which seeks to make the generated MTS designs indistinguishable from the training data set. The adversarial training between G and D hits several points of instability before settling into regions of local equilibrium as the number of training epochs increases. Performance may continue to improve with more training epochs (iterations). MTS unit cell design image results generated by the DC-GAN are shown in Fig. 6. As training iterations increase, the generated MTS unit cell designs begin to resemble design features seen in the training data set. It is expected that the generated images will continue to improve and become crisper with more training iterations. Post-processing image smoothing and filtering is performed to reduce image background noise and realize a practical design. Additional hyperparameter tuning and larger training data set could improve the results further.

Figure 7 details the validation results for an example meta-atom design test case. Figure 7a shows the meta-atom design geometry

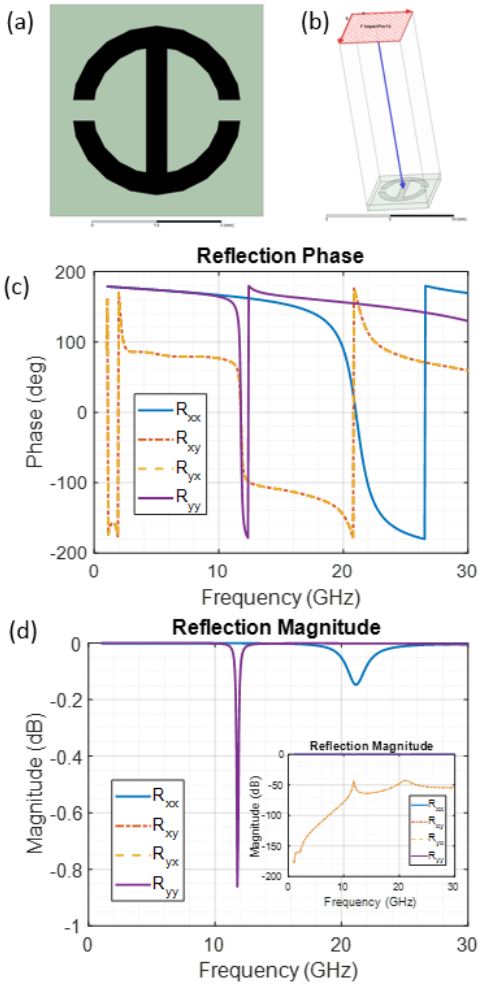

Fig. 4. Simulated reflected magnitude and phase for example MTS unit cell in training data set. (a) Unit cell design. (b) Unit cell simulation set-up in HFSS with Floquet port excitation and periodic boundary conditions. (c) Simulated reflection phase of the MTS unit cell. (c) Simulated reflection magnitude of the MTS unit cell.

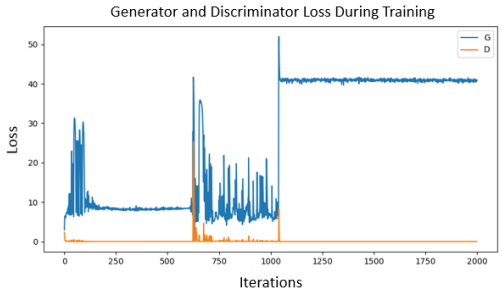

Fig. 5. Loss functions of DC-GAN generator (G) and discriminator (D) networks during training.

chosen for the validation test case. The post-processed generated image (Fig. 7b) closely resembles the test case geometry of Fig 7a. The magnitude (phase) response of the test case generated using full-wave simulation is shown in Fig. 7c (Fig. 7e). The corresponding full-wave EM magnitude (phase) response for the DC-GAN generated output in Fig. 7b are plotted in Fig. 7d (Fig. 7e). In each of the

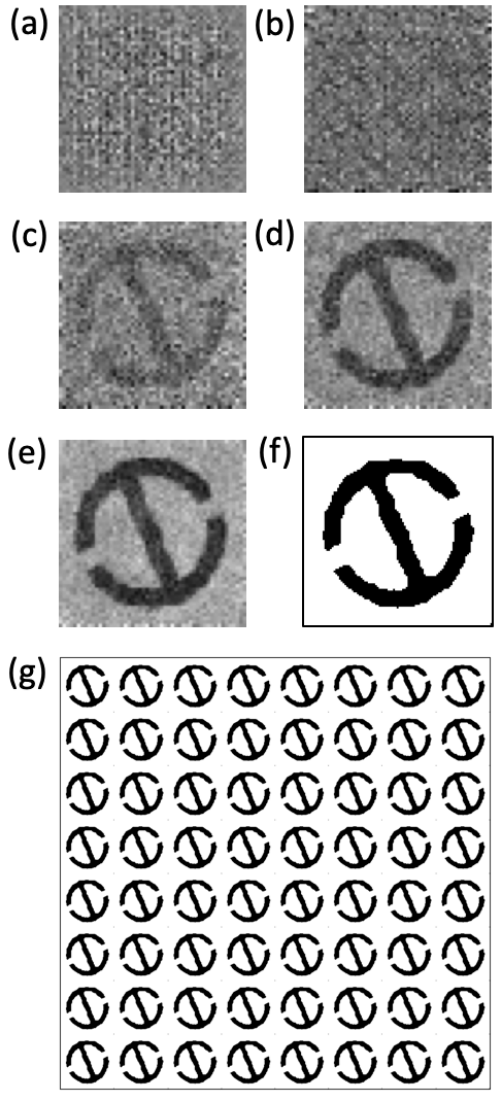

Fig. 6. Generated images from the DC-GAN network after (a) 1 training epoch, (b) 500 training epochs, (c) 750 training epochs, (d) 1000 training epochs, and (e) 2000 training epochs. (f) Image filtering is performed during post-processing to reduce noise so that a more practical design is realized. (g) Example 8-by-8 element MTS array using meta-atom design generated in (a-f). In practice, the design at each row in pixel varies.

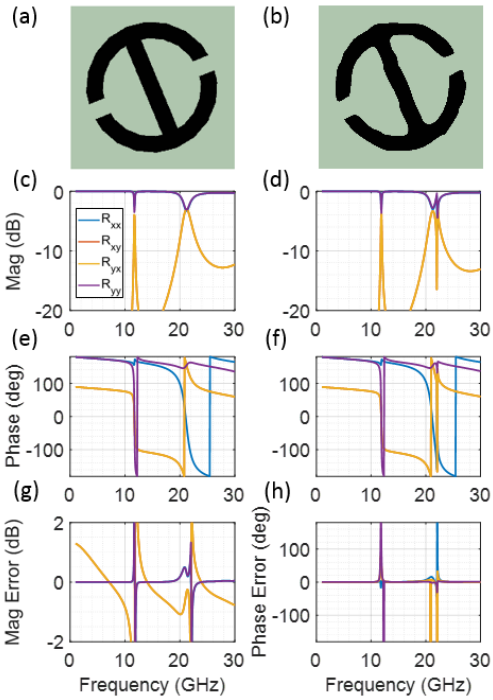

Fig. 7. Validation results for an example meta-atom design test case. (a) Meta-atom design geometry chosen for validation test case consisting of PEC (black) and dielectric (turquoise). (b) Generated design geometry using DC-GAN based on response of test case. (c) Desired reflection magnitude response of the test case in (a). (d) Reflection magnitude response of the generated shape in (b). (e) As in (c), but now the phase response is depicted. (f) As in (d),but now the phase response is depicted. (g) Difference between the reflection magnitude response of the generated meta-atom geometry and the test case geometry. (h) As in (g), but for the phase response.

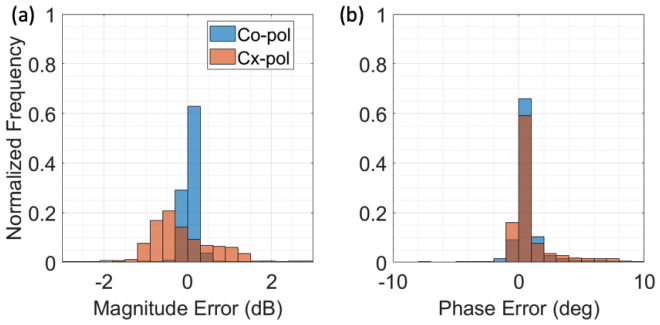

Fig. 8. Distribution of errors computed in Fig. 7g and h for (a) magnitude and (b)phase responses, respectively. Co-polarization (co-pol) are defined as R_{xX} and R_{yy}. Similarly, cross-polarization (cx-pol) components are defined as R_{xy} and R_{yx}.

Figs. 7c-h, the spectral response line of R_{yx} is overlaid by R_{xy}. Note that the spectral response R_{xx} is not visible in these plots because it is overlaid with R_{yy} curve.

We compared the reflection magnitude and phase responses of the generated meta-atom in Figs. 7d and f with their desired spectral responses in Figs. 7c and e. The histogram of errors in the responses are depicted in Figs. 8. The errors in reflection magnitude and phase are centered near zero and fall within acceptable bounds for many applications for most frequency points. For this example test case, the generated response is in close agreement for most frequency points. In particular, we obtain an accuracy of 90% for reflection responses within ± 0.2 dB in magnitude and $\pm 3.0^{\circ}$ in phase for the co-pol components (R_{xx} and R_{yy}). The corresponding values for the cx-pol components (R_{xy} and R_{yx} are ± 1.3 dB and $\pm 4.4^{\circ}$. The results become more robust and generalizable using a larger training data.

V. Summary

We proposed and validated a DL approach to aid the design of RF MTSs. Specifically, by training a DC-GAN on an image data set of known MTS unit cell designs, the algorithm is able to generate new MTS designs from the learned design data distribution. Results from this study show promise of DC-GANs to reduce design time while also obtaining high accuracy in terms of multiple design parameters such as magnitude, phase and various polarization responses. Future work will focus on using improved hardware (GPUs) to train the DC-GAN for more iterations to achieve more robust results.

978-1-7281-3049-1/19/$31.00 ©2019 IEEE

Acknowledgements

J. A. H. acknowledges support from Northrop Grumman Mission Systems (NGMS), Baltimore, MD, for his thesis research. K. V. M. acknowledges support from the National Academies of Sciences, Engineering, and Medicine via Army Research Laboratory Harry Diamond Distinguished Postdoctoral Fellowship.

References

[1] J. A. Hodge, T. Anthony, and A. I. Zaghloul, "Enhancement of the dipole antenna using a capcitively loaded loop (CLL) structure," in *IEEE Antennas and Propagation Society International Symposium*, 2014, pp. 1544–1545.

[2] Q. M. Nguyen, K. V. Mishra, and A. I. Zaghloul, "Retrieval of polarizability matrix for metamaterials," in *IEEE International Conference on Microwaves, Communications, Antennas and Electronic Systems*, 2019, submitted.

[3] S. B. Glybovski, S. A. Tretyakov, P. A. Belov, Y. S. Kivshar, and C. R. Simovski, "Metasurfaces: From microwaves to visible," *Physics Reports*, vol. 634, pp. 1–72, 2016.

[4] H.-T. Chen, A. J. Taylor, and N. Yu, "A review of metasurfaces: physics and applications," *Reports on Progress in Physics*, vol. 79, no. 7, p. 076401, 2016.

[5] D. R. Smith, O. Yurduseven, L. P. Mancera, P. Bowen, and N. B. Kundtz, "Analysis of a waveguide-fed metasurface antenna," *Physical Review Applied*, vol. 8, no. 5, p. 054048, 2017.

[6] K. V. Mishra, J. A. Hodge, and A. I. Zaghloul, "Reconfigurable metasurfaces for radar and communications systems," in *URSI Asia-Pacific Radio Science Conference*, 2019, pp. 1–4.

[7] S. D. Campbell, D. Sell, R. P. Jenkins, E. B. Whiting, J. A. Fan, and D. H. Werner, "Review of numerical optimization techniques for meta-device design," *Optical Materials Express*, vol. 9, no. 4, pp. 1842–1863, 2019.

[8] W. Ma, F. Cheng, and Y. Liu, "Deep-learning enabled on-demand design of chiral metamaterials," *ACS Nano*, 2018.

[9] Y. LeCun, Y. Bengio, and G. Hinton, "Deep learning," *Nature*, vol. 521, no. 7553, p. 436, 2015.

[10] I. Goodfellow, Y. Bengio, and A. Courville, *Deep Learning*. MIT Press, 2016.

[11] A. M. Elbir and K. V. Mishra, "Deep learning design for joint antenna selection and hybrid beamforming in massive MIMO," in *IEEE International Symposium on Antennas and Propagation*, 2019, in press.

[12] ——, "Joint antenna selection and hybrid beamformer design using unquantized and quantized deep learning networks," *arXiv preprint arXiv:1905.03107*, 2019.

[13] S. Inampudi and H. Mosallaei, "Neural network based design of metagratings," *Applied Physics Letters*, vol. 112, no. 24, p. 241102, 2018.

[14] J. Jiang, D. Sell, S. Hoyer, J. Hickey, J. Yang, and J. A. Fan, "Data-driven metasurface discovery," *arXiv preprint arXiv:1811.12436*, 2018.

[15] D. Liu, Y. Tan, E. Khoram, and Z. Yu, "Training deep neural networks for the inverse design of nanophotonic structures," *ACS Photonics*, vol. 5, no. 4, pp. 1365–1369, 2018.

[16] J. Peurifoy, Y. Shen, L. Jing, Y. Yang, F. Cano-Renteria, B. G. DeLacy, J. D. Joannopoulos, M. Tegmark, and M. Soljačić, "Nanophotonic particle simulation and inverse design using artificial neural networks," *Science Advances*, vol. 4, no. 6, p. eaar4206, 2018.

[17] I. Malkiel, M. Mrejen, A. Nagler, U. Arieli, L. Wolf, and H. Suchowski, "Deep learning for the design of nano-photonic structures," in *IEEE International Conference on Computational Photography*, 2018, pp. 1–14.

[18] Q. Zhang, C. Liu, X. Wan, L. Zhang, S. Liu, Y. Yang, and T. J. Cui, "Machine-learning designs of anisotropic digital coding metasurfaces," *Advanced Theory and Simulations*, p. 1800132, 2018.

[19] I. Goodfellow, J. Pouget-Abadie, M. Mirza, B. Xu, D. Warde-Farley, S. Ozair, A. Courville, and Y. Bengio, "Generative adversarial nets," in *Advances in Neural Information Processing Systems 27*, 2014, pp. 2672–2680.

[20] Z. Liu, D. Zhu, S. P. Rodrigues, K.-T. Lee, and W. Cai, "Generative model for the inverse design of metasurfaces," *ACS Nano Letters*, vol. 18, no. 10, pp. 6570–6576, 2018.

[21] A. Radford, L. Metz, and S. Chintala, "Unsupervised representation learning with deep convolutional generative adversarial networks," in *International Conference on Learning Representations*, 2016, pp. 1–16.

[22] J. A. Hodge, K. V. Mishra, and A. I. Zaghloul, "Reconfigurable metasurfaces for index modulation in 5G wireless communications," in *IEEE International Applied Computational Electromagnetics Society Symposium*, 2019, pp. 1–2.

[23] J. A. Hodge and A. I. Zaghloul, "Utilizing a reconfigurable metasurface antenna as a device for spatial multiplexing and modulation," in *URSI Radio Science Meeting*, 2018.

[24] ——, "Towards addressable and reconfigurable metasurfaces: Utilizing active and passive variants of the capacitive-loaded loop (CLL) element for the design of modulated metasurface antennas," in *URSI Radio Science Meeting*, 2017.

[25] K. Chen, Y. Feng, F. Monticone, J. Zhao, B. Zhu, T. Jiang, L. Zhang, Y. Kim, X. Ding, S. Zhang *et al.*, "A reconfigurable active Huygens' metalens," *Advanced Materials*, vol. 29, no. 17, 2017.

[26] X. Wan, M. Q. Qi, T. Y. Chen, and T. J. Cui, "Field-programmable beam reconfiguring based on digitally-controlled coding metasurface," *Scientific Reports*, vol. 6, p. 20663, 2016.

[27] M. Mirza and S. Osindero, "Conditional generative adversarial nets," *arXiv preprint arXiv:1411.1784*, 2014.

[28] N. Inkawhich, "DCGAN tutorial," accessed 2019-07-12. [Online]. Available: https://pytorch.org/tutorials/beginner/dcgan_faces_tutorial.html

[29] H.-T. Chen, "Interference theory of metamaterial perfect absorbers," *Optics Express*, vol. 20, no. 7, pp. 7165–7172, 2012.

[30] D. Schurig, J. J. Mock, and D. R. Smith, "Electric-field-coupled resonators for negative permittivity metamaterials," *Applied Physics Letters*, vol. 88, no. 4, p. 041109, 2006.

[31] P. Su, Y. Zhao, S. Jia, W. Shi, and H. Wang, "An ultra-wideband and polarization-independent metasurface for RCS reduction," *Scientific Reports*, vol. 6, p. 20387, 2016.

[32] A. T. Pereda, F. Caminita, E. Martini, I. Ederra, J. C. Iriarte, R. Gonzalo, and S. Maci, "Dual circularly polarized broadside beam metasurface antenna," *IEEE Transactions on Antennas and Propagation*, vol. 64, no. 7, pp. 2944–2953, 2016.

[33] G. Minatti, M. Faenzi, E. Martini, F. Caminita, P. De Vita, D. González-Ovejero, M. Sabbadini, and S. Maci, "Modulated metasurface antennas for space: Synthesis analysis and realizations," *IEEE Transactions on Antennas and Propagation*, vol. 63, no. 4, pp. 1288–1300, 2015.

[34] S. Sun, Q. He, S. Xiao, Q. Xu, X. Li, and L. Zhou, "Gradient-index meta-surfaces as a bridge linking propagating waves and surface waves," *Nature Materials*, vol. 11, no. 5, pp. 426–431, 2012.

[35] Q. M. Nguyen and A. I. Zaghloul, "Impedance matching metamaterials composed of ELC and NB-SRR," in *IEEE Antennas and Propagation Society International Symposium*, 2018.

[36] M. Mencagli, E. Martini, and S. Maci, "Surface wave dispersion for anisotropic metasurfaces constituted by elliptical patches," *IEEE Transactions on Antennas and Propagation*, vol. 63, no. 7, pp. 2992–3003, 2015.

[37] B. H. Fong, J. S. Colburn, J. J. Ottusch, J. L. Visher, and D. F. Sievenpiper, "Scalar and tensor holographic artificial impedance surfaces," *IEEE Transactions on Antennas and Propagation*, vol. 58, no. 10, pp. 3212–3221, 2010.

[38] J. Su, Y. Lu, H. Zhang, Z. Li, Y. L. Yang, Y. Che, and K. Qi, "Ultra-wideband, wide angle and polarization-insensitive specular reflection reduction by metasurface based on parameter-adjustable meta-atoms," *Scientific Reports*, vol. 7, p. 42283, 2017.

[39] A. Paszke, S. Gross, S. Chintala, G. Chanan, E. Yang, Z. DeVito, Z. Lin, A. Desmaison, L. Antiga, and A. Lerer, "Automatic differentiation in PyTorch," in *Conference on Neural Information Processing Systems: Autodiff Workshop*, 2017, pp. 1–4.

[40] D. P. Kingma and J. Ba, "Adam: A method for stochastic optimization," *arXiv preprint arXiv:1412.6980*, 2014.